High-resolution photoelectron emission spectroscopy of surface states on Ni(111)

J. Kutzner, R. Paucksch,* C. Jabs, and H. Zacharias
Physikalisches Institut, Westfälische Wilhelms-Universität Münster, D-48149 Münster, Germany

J. Braun
Fachbereich Physik, Universität Osnabrück, D-49069 Osnabrück, Germany

(Received 23 June 1997)

One-photon and two-photon photoelectron emission (1PPE/2PPE) spectroscopy is used to study surface states at and below the Fermi energy on Ni(111) in $\Gamma\rightarrow K$ and $\Gamma\rightarrow M$ direction. Picosecond UV laser pulses at $\lambda=210.70$ nm ($\tilde{\nu}=47\,460.16$ cm^{-1}) and $\lambda=351.17$ nm ($\tilde{\nu}=28\,476.09$ cm^{-1}) are used for photoexcitation. The energy of the emitted photoelectrons is analyzed in a time-of-flight spectrometer with an energy resolution of $\Delta E<20$ meV. Two surface states located below the Fermi energy and energetically separated by 120 meV are detected at Γ. With increasing $k_{\|}$ the high-energy state disperses upwards, while the low-energy state disperses downwards. Furthermore, a theoretical investigation is performed in the framework of the relativistic one-step formalism. The measured surface-state dispersions are shown to be quantitatively described by the calculations. For the relative and absolute intensities of the two surface states at and around Γ experiment and theory are not in agreement. [S0163-1829(97)06147-X]

I. INTRODUCTION

Surface states (SS's) play an important role in a variety of processes on metal surfaces. Recent experiments show their importance in reconstruction effects,[1] nonadiabatic damping of adsorbate vibrations,[2] and adsorbate-adsorbate interactions.[3,4] Furthermore, surface states contribute to the nonlinear optical response of surfaces,[5] and influence the surface magnetism.[6–12] In the past, surface states on Ni(111) have drawn considerable attention. In early angle-resolved photoelectron spectroscopy investigations, Eastman and Himpsel[13] found an occupied, nonmagnetic, totally symmetric Λ_1 surface state at $E_B=-0.25$ eV binding energy, which disperses downwards with increasing $k_{\|}$. In conventional[14] and spin-resolved inverse photoemission studies,[7] a partially occupied Λ_1 surface state just at E_F is reported. This state disperses upwards with increasing $k_{\|}$. The spin-resolved measurements reveal a magnetic exchange splitting of about $\Delta E=100$ meV, and the detected state is assumed to be derived from the p-like $L_{2'}$ bulk state. Borstel *et al.*[15] performed a numerical calculation which yielded only one surface state at Γ which splits into two components for nonzero $k_{\|}$. Bertel[16] obtained the same result when applying a theoretical symmetry analysis to the surface state close to E_F. He supposed that slight misalignments or residual contaminations of the sample cause a small energy difference between the photoemission and inverse photoemission results at Γ.

In the literature, the existence of one or two surface states at Γ thus remains disputed. In photoemission studies only occupied states, and in inverse-photoemission experiments only unoccupied states, are detectable. Both methods thus yield complementary information. Only at E_F is a certain overlap present. The Λ_1 surface state reported by Eastman and Himpsel is not accessible by the inverse photoemission (IPE) method. The comparatively low energy resolution of about 100 meV of earlier photoelectron investigations, and the chosen photon energies, did not permit an observation of two separated surface states at Γ on the Ni(111) surface. In this study we report one- and two-photon spin-averaged photoemission measurements on Ni(111) using UV laser radiation with a picosecond pulse duration. The energy spread of the photon source is about 0.50 cm^{-1} ($\lambda=351$ nm) and 0.64 cm^{-1} ($\lambda=211$ nm). The photoelectron emission from states near E_F is studied with an energy resolution of better than $\Delta E=20$ meV.

II. EXPERIMENT

The experiments are performed in an ultrahigh-vacuum chamber with a base pressure of 2×10^{-10} mbar. A retarding field Auger spectrometer and low-energy electron diffraction (LEED) are used to ensure the cleanliness and order of the surface. For an additional check of the cleanliness of the prepared surface, photoemission using coherent vacuum ultraviolet laser radiation generated by frequency conversion in rare gases was also used.[17] The nickel crystal is mounted on a liquid-nitrogen-cooled molybdenum plate, and could be radiatively heated to 1050 K. The Ni(111) sample is initially prepared by repeated cycles of Ar^+-ion sputtering and heating (up to 1050 K), together with an oxygen treatment to remove sulfur and carbon from the sample. Before each run it is cleaned again at low Ar^+-ion current, and is then subsequently annealed.

The ultraviolet radiation for photoemission is derived from a Nd:YLF (neodymium: yttrium lithium fluorid) laser system. It consists of a mode-locked oscillator and a regenerative amplifier operating at 76 MHz and 1 kHz, respectively. Laser pulses of 70-ps duration and about 2.5-mJ energy are emitted at a measured infrared wavelength of $\lambda_{vac}=1053.50$ nm. Consecutive frequency doubling in a $LiBO_3$ crystal and sum-frequency mixing in a second $LiBO_3$ crystal yields strictly linearly polarized UV radiation at $\lambda_{vac}=351.17$ nm ($h\nu=3.53$ eV, $\tilde{\nu}=28\,476.09$ cm^{-1}) with a

pulse energy of up to 350 μJ and a pulse duration of 40 ps. This 351-nm radiation is used for the two-photon photoemission (2PPE) measurements. The polarized UV laser beam is incident on the sample under an angle of 60° with respect to the surface normal, and is focused by a quartz lens ($f=500$ mm). The measured beam radius is $w=100$ μm at the position of the Ni(111) surface. Under these conditions the irradiated elliptical spot has an area of about 6×10^{-4} cm^2 on the sample. Pulse energies of 4 μJ resulting in fluences of about 6 mJ/cm^2 have been applied to the nickel crystal to avoid space charge broadening effects. About 0.2 electrons per laser pulse have been detected under these conditions. The fifth harmonic of the neodym laser at $\lambda_{vac}=210.70$ nm is generated by frequency doubling the second harmonic in a β-BaB_2O_3 crystal, yielding UV radiation at $\lambda_{vac}=263.35$ nm ($h\nu=4.71$ eV, $\tilde{\nu}=37\,971.73$ cm^{-1}) with a pulse energy of up to 250 μJ and a pulse duration of 35 ps. Sum frequency mixing of this radiation with the fundamental radiation in a second β-BaB_2O_3 crystal yields 210.70 nm ($\tilde{\nu}=47\,460.16$ cm^{-1}) radiation. At this wavelength, pulses of 10 μJ at a duration of 31 ps are available at the surface for one photon photoemission (1PPE). For the highly efficient 1PPE process the intensity of the 211-nm radiation has to be attenuated by several orders of magnitude to reduce the number of emitted photoelectrons in order to avoid space-charge-induced broadening effects.

The emitted photoelectrons are detected in a time-of-flight (TOF) electron spectrometer with a sample-detector distance of 879 mm. The geometric collection angle of the emitted electrons is $\pm1.3°$ along the surface normal. The electrons are detected by microchannel plates (MCP's) with an impedance matched 50-Ω anode. The MCP signal is recorded by a 1 GHz time-to-digital-converter which is directly connected to the internal bus of a VME bus computer (Eltec). The energy resolution of the spectrometer, which depends on the kinetic energy of the detected electrons, is determined to $\Delta E=16$ meV at 2 eV kinetic energy by nonresonant three-photon ionization of xenon in the gas phase using 263-nm radiation.

The measured time-of-flight distributions $N(t)dt$ are directly transformed into kinetic-energy distributions, $N(E)dE$. A transformation from the time to the energy scale has to conserve the total particle number, thus $N(E)dE=N(t)dt$. For a constant flight path L and constant velocity in a field-free drift tube, the kinetic energy is given by $E=(m/2)(L/t)^2$, yielding $|dE/dt|=mL^2/t^3$ for the Jacobian. Combining these equations yields $N(E)=t^3N(t)/(mL^2)$ for the transformation. L is the overall flight path, m the electron mass, and t the flight time of the electrons. From the zero-kinetic-energy edge in this spectrum, the work-function difference between sample and electron spectrometer is determined. In the present case the electrons experience an accelerating potential of 0.99 V between the Ni(111) sample and the spectrometer. Using this value corrected kinetic-energy distributions of the emitted photoelectrons at the sample surface are generated numerically. The simulated electric-field distribution between the sample and TOF entrance is included in this numerical simulation. Differences between the direct transformation and the numerical simulation turn out to be small (1–3 meV). When turning the sample in front of the spectrometer the changing electrical field conditions have also been taken into account. Due to the accelerating potential the angular resolution is reduced to $\pm2.7°$ for normal emission and to $\pm3.8°$ for emission at 15° off-normal at E_F when using 211-nm radiation. In the case of the two-photon emission with 351-nm radiation, the angular resolution at E_F is $\pm2.5°$ for normal emission and $\pm3.5°$ for 15° off-normal detection.

III. THEORY

In this section the key aspects of relativistic photoemission theory will be outlined. Based on the one-step model,[18,19] the relativistic generalization of the photocurrent allows the calculation of spin-integrated and spin-resolved photoemission spectra for pure elemental solids.[20–22] Within a relativistic one-step theory the photocurrent for photoelectrons with energy ε_f and momentum $\mathbf{k}_\parallel$ parallel to the surface is described by the spin-density matrix ρ. In the space representation, one can write

$$\rho(\varepsilon_f,\mathbf{k}_\parallel)=-\frac{1}{\pi}\,\mathrm{Im}\int d\mathbf{r}\int d\mathbf{r}'\,\Psi_f^\dagger(\mathbf{r})\times\Delta G_1^+(\mathbf{r},\mathbf{r}')\Delta^\dagger\Psi_f(\mathbf{r}'). \tag{1}$$

Herein $\Psi_f^\dagger(r)$ describes the time-reversed spin-polarized LEED (SPLEED) state

$$\Psi_f^\dagger(\mathbf{r})=\langle\mathbf{r}|G_2^+|\varepsilon_f,\mathbf{k}_\parallel\rangle. \tag{2}$$

For all further derivations, atomic units ($\hbar=e=m=1$, $c=137.036$) will be used. Further, the positive z-axis points inside the semi-infinite crystal. The final and initial state propagators $G_2^\pm$ and G_1^+, respectively, can be expressed by 4×4 matrices, and the time-reversed SPLEED state $\Psi_f^\dagger(r)$ takes the form of a four-component Dirac spinor. In the relativistic theory the interaction of an electron with the electromagnetic field is described by the operator

$$\Delta=-\boldsymbol{\alpha}\cdot\mathbf{A}_0, \tag{3}$$

with the spatially constant amplitude $\mathbf{A}_0$ of the electromagnetic vector potential. The three components α_k of the vector $\boldsymbol{\alpha}$ are defined through the tensor product $\alpha_k=\sigma_1\otimes\sigma_k$, $k=1,2,3$, where σ_k denote the Pauli spin matrices. The spin-averaged photocurrent I and the z component p_z of the spin polarization vector $\mathbf{p}$ are then obtained from

$$I=\mathrm{tr}(\rho) \tag{4}$$

and

$$p_z=\frac{\mathrm{tr}(\sigma_z\rho)}{\mathrm{tr}(\rho)}, \tag{5}$$

with the z component σ_z of the Pauli spin operator σ. For further details see Refs. 20–22.

IV. RESULTS AND DISCUSSION

One-photon photoelectron emission spectroscopy is performed with UV laser radiation at $\lambda=210.70$ nm ($h\nu=5.884$ eV and 2PPE spectroscopy with 351.17 nm ($h\nu=3.531$ eV) radiation. Figure 1 shows energy distribution

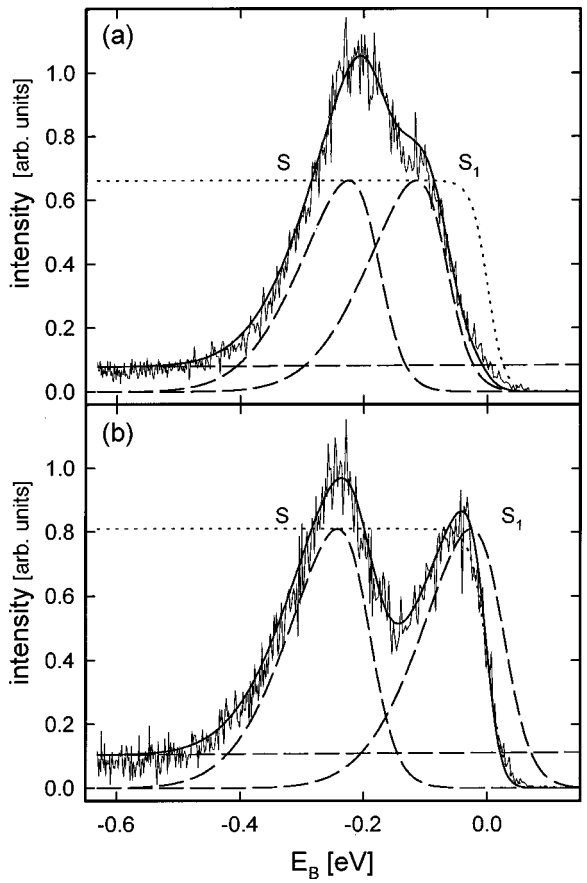

FIG. 1. One-photon photoelectron emission spectra of Ni(111) at $\lambda \sim 211$ nm. The energy resolution at the Fermi energy ($E_B = 0$ eV) is 13 meV, and the sample temperature $T = 140$ K. (a) Energy distribution curve (EDC) obtained for normal emission (at $\bar{\Gamma}$). (b) EDC obtained for off-normal emission at $\theta = 5°$ in the $\bar{\Gamma} \rightarrow K$ direction. In both spectra the measured signal intensity is fitted by a function considering the electron spectrometer resolution, the Fermi distribution function (dotted), the bulk emission, and two surface states. The two surface states as well as the bulk contribution obtained from the fit are shown separately by the dashed lines. The details are described in the text.

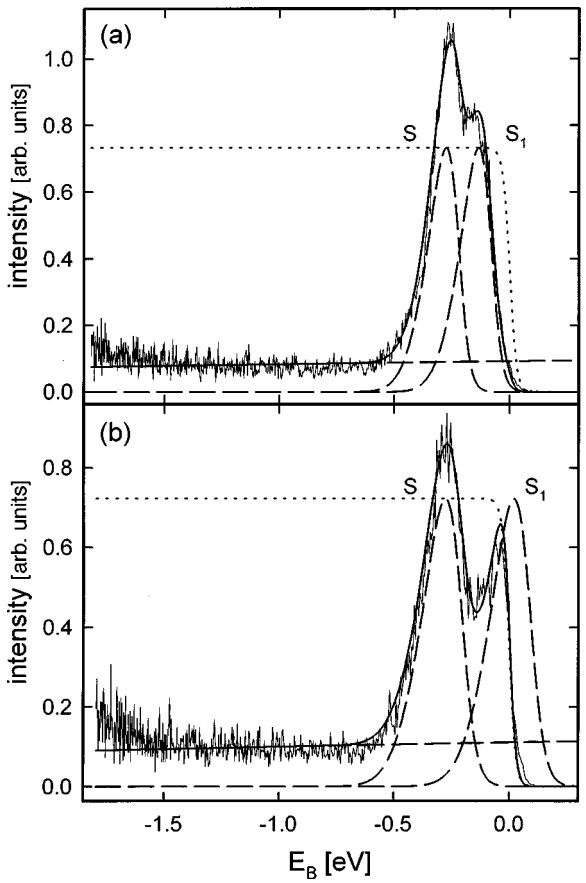

FIG. 2. Two-photon photoelectron emission spectra of Ni(111) at $\lambda = 351$ nm showing EDC's at $\theta = 0°$ (a) and $\theta = 5°$ (b). Due to the higher two-photon energy of 7.06 eV, a larger part of the nickel $3d$ band can be seen. Despite a lower-energy resolution of 29 meV at $E_B = 0$ eV, results comparable to the 1PPE spectra are obtained with the 2PPE technique.

curves (EDCs) obtained with p-polarized light at $\lambda \sim 211$ nm. At the Fermi edge position ($E_B = 0$ eV) the resolution of the spectrometer is about 13 meV. The spectrum cuts off at $E_B = -0.65$ eV, which yields a Ni(111) work function of $\phi = 5.23$ eV in accordance with earlier work.[23,24] Experimental points of the Ni energy bands given in Ref. 25 are $L_{3\uparrow} = -0.15$ eV (with respect to $E_F = 0$ eV), $L_{3\downarrow} = +0.16$ eV, and $L_1 = +6.0$ eV. Thus, using the 211-nm radiation ($h\nu = 5.88$ eV), only indirect transitions from $\Lambda_{3\uparrow}$ and $\Lambda_{3\downarrow}$ into evanescent Λ_1 states can be excited. The photoelectron spectrum thus reflects the density of states of both $\Lambda_{3\uparrow}$ and $\Lambda_{3\downarrow}$, but the intensity is expected to be weak. The emission from surface states is superimposed on the intensity from these bulk bands. Photoelectrons derived from surface states couple to plane waves in the vacuum in a single step which is significantly less restrictive than for the bulk. As a result, emission from surface states should dominate. Experiments with $h\nu \sim 6$ eV radiation, as in the present work, should thus be most effective to discriminate between bulk and surface contributions, since these photoelectron emission spectra should be dominated by surface-state emission and not be complicated by the presence of additional bulk transitions.

In a high-resolution spectrum taken off-normal ($\theta = 5°$), clearly two separated signal peaks appear [Fig. 2(b)] at about $E_B = -0.25$ eV denoted by S, and around E_F, denoted by S_1. The energetic position of the former state (S) is in accordance with the Λ_1 surface resonance reported by Eastman and co-workers.[13,25] The other state, labeled S_1, is cut off by the Fermi function. It is only partially occupied and thus only partly visible in the spectrum. Its energetic position coincides with the resonance reported in inverse-photoemission studies.[7,9,14] In normal emission the separation of the two states is not as obvious [Fig. 2(a)], although here a shoulder at $E_B = -0.1$ eV is also clearly discernible. We therefore conclude that two surface states exist at $\bar{\Gamma}$. In addition, no significant signal intensity is detected at the Fermi energy, showing clearly that *both* surface states are located completely below E_F. One thus may conclude that S_1 is nonmagnetic at $\bar{\Gamma}$. IPE results, however, suggest that the high-energy state S_1 is only partially occupied and magnetic at $\bar{\Gamma}$.[7] The existence of S_1 at $\bar{\Gamma}$ reveals it as a true surface state in a symmetry gap at $\bar{\Gamma}$, since mixing with bulk states of same energy and symmetry is no longer possible. As pointed out in

Ref. 7, it is derived from the p-like L_2 point rather than the d-like L_3 point. To analyze the signal structure in more detail with regard to quantitative results, a simplified model is used to describe the measured photoelectron signal. Therein the signal structure is a superposition of the (weak) bulk emission and the emission from two surface states (see the dashed lines in Fig. 2). The three-dimensional free-electron-gas model is used to describe the bulk contribution. In case of the surface states we assume that both states have the same peak intensity I_0 and signal form $I(E)$ and are described by a Gaussian function of the form

$$I(E)=A(E)\frac{I_0}{\sqrt{2\pi\sigma}}\exp\left[-\frac{1}{2}\left(\frac{E-E_0}{\sigma}\right)^2\right], \tag{6}$$

with the factor

$$A(E)=\frac{2}{1+\exp[B(E-E_0)]}. \tag{7}$$

In this expression σ is the Gauss width, I_0 the peak intensity, and E_0 the energetic position of the pure Gaussian peak, which slightly differs from the overall signal peak. $A(E)$ is a factor that takes the asymmetric form of the SS signals into account. This asymmetry is described by the factor B. The resolution of the electron spectrometer, as well as the influence of the Fermi distribution function (dotted line), have been considered. Applying this model to the experimental data yields the continuous lines in Fig. 1 as a fit result. The dashed lines denote the single components, i.e., the bulk contribution and the two surface states, for both normal and off-normal emission. The Fermi distribution function convoluted with the apparatus function is also shown (dotted line). The energetic positions of the surface states at $\bar{\Gamma}$ have been determined from these fits to $E_B=(-0.230\pm0.015)$ eV for the lower-energy state S, and $E_B=(-0.110\pm0.020)$ eV for the higher-energy state S_1. The given uncertainties have been deduced from the statistics, and do not include systematic errors due to the chosen fit functions and assumptions. An energy gap of about 120 meV is found from a single spectrum between S and S_1 at $\bar{\Gamma}$. The deduced width for a single surface state at $\bar{\Gamma}$ is (160 ± 10) meV [full width at half maximum (FWHM)]. In other experiments with a lower energy resolution an overall width (including both surface states) of $\sim$300 meV (FWHM) is reported.[13,24]

Figure 2 shows two-photon photoelectron emission spectra obtained with p-polarized radiation at $\lambda=351$ nm. Due to the higher two-photon energy of 7.06 eV this spectrum cuts off at $E_B=-1.83$ eV. Direct transitions from Λ_3 to Λ_1 are now possible because of $2h\nu>L_1$.[25] Due to the higher kinetic energy of the emitted photoelectrons the energy resolution at $E_B=0$ eV is reduced to $\Delta E\sim29$ meV. Concerning the two surface states the 2PPE method yields similar results to the 1PPE method. An additional significant contribution of the bulk emission is not obvious at a first glance. However, a slightly increased gap of about 130 meV between both SS's and an increased width of about 180 ± 20 meV for a single SS component is obtained at $\bar{\Gamma}$ caused by a lower energy and $k_\parallel$ resolution, and probably the influence of bulk emission.

The dispersion of the surface resonances has been determined by tilting the sample. Figure 3 shows 1PPE spectra for

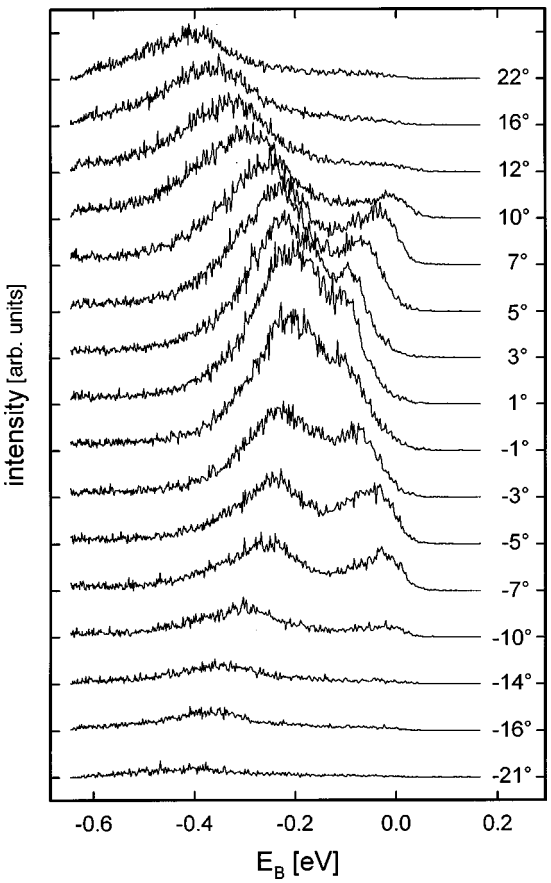

FIG. 3. Experimental dispersion of surface states along $\bar{\Gamma}\rightarrow\bar{K}$ direction for $h\nu=5.88$ eV radiation. 1PPE spectra of Ni(111) taken with 211-nm p-polarized radiation for various emission angles are shown. The sample temperature is $T=155$ K.

p-polarized 211-nm light and various emission angles in the $\bar{\Gamma}\rightarrow\bar{K}$ direction. A downward shift of S and an upward shift of S_1 above E_F is observed when increasing $k_\parallel$. The experimental data reveal that the intensity of S has a maximum at $\bar{\Gamma}$. For increasing $k_\parallel$ the intensity decreases. For S_1, which is only partly occupied for finite $k_\parallel$, no definite statement about the intensity can be made from the photoelectron emission data. However, the chosen assumptions in the fit model about form and intensity of the two SS's appear to be reasonable, and are based on the fact that both surface-state signals have approximately the same height when they can be seen separately in the spectra.

Figure 4 shows theoretical photoemission spectra for various emission angles θ in the $\bar{\Gamma}\rightarrow\bar{K}$ direction. A paramagnetic muffin-tin potential from Ref. 26 was used, together with a surface barrier of Rundgren-Malmström type,[27] in order to describe the crystal potential. Furthermore, the parametrized surface barrier was optimized by comparison with the experimental photoemission data. Possible damping processes were considered in a phenomenological way by adding an imaginary contribution $-iV_{oi}$ to the muffin-tin potential of Ni. The initial state V_{oi} was chosen to $V_{oi}=0.03$ eV. The corresponding value for the final state, which was used in the theoretical investigation, is $V_{oi2}=1.0$ eV. The most striking observation in the calculated photoemission spectra of Fig. 4 is that the intensity of S_1 appears to be much higher than that

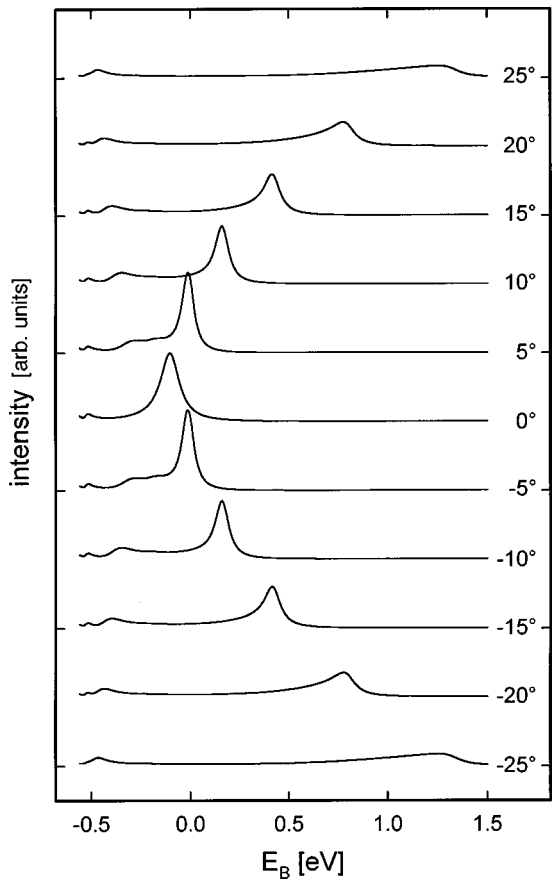

FIG. 4. Theoretical curves calculated with the relativistic one-step model. The intensity of the low-energy state S is small in comparison with S_1, and decreases completely when approaching Γ ($\theta = 0°$).

of S. In disagreement to the experimental data, the intensity of S decreases with decreasing $k_\parallel$, and approaches zero at the Γ point. The existence of more than one surface state at Γ cannot be supported by the relativistic one-step model by changing the parameters. We also considered surface corrugation effects, but no intensity of S could be generated at Γ. Former one-step model calculations performed by Borstel *et al.*[15] came to the same result. However, in their calculation the S_1 state terminated at the bulk band edge, i.e., only S existed at Γ.

The results of a detailed analysis of the experimental as well as of the calculated $k_\parallel$ dispersion of surface states on Ni(111) in $\Gamma \rightarrow K$ and $\Gamma \rightarrow M$ directions of the surface Brillouin zone are shown in Fig. 5. Due to the low kinetic energy of the photoelectrons emitted, only a small $k_\parallel$ interval around Γ can be projected by tilting the sample in an angle interval of $+25° \leqslant \theta \leqslant -25°$. We restricted our analysis to values of $|k_\parallel| \leqslant 0.15$ Å^{-1}. The data points given are extracted from fits of the observed photoelectron intensities by the above discussed model. It should be pointed out again that the experimental data points given for the S state are based on the easily obtainable data, which are directly accessible by photoelectron spectroscopy. In contrast, the data points given for the upward dispersing S_1 state are much more strongly dependent on the fit procedure used. This fit is based on the assumption of the same intensity of both SS's for fixed $k_\parallel$, and the same widths of both Gaussian line shapes. With increasing $k_\parallel$, S disperses downwards in energy, while S_1 disperses upwards and crosses the Fermi energy at about $k_\parallel = 0.06$ Å^{-1}. The one-photon results (filled circles) agree with the two-photon results (filled squares) within the experimental uncertainty. However, slight deviations between both data sets are noticeable, most obviously in the $\Gamma \rightarrow K$ direction. They are probably caused by additional bulk emission, which is not included in the applied model in the case of the higher two-photon energy. The continuous lines represent parabolic fits taking both 1PPE and 2PPE results into account. They describe free-electron-like dispersions with effective electron masses of $m^*/m = (-0.41 \pm 0.2)$ for S, and $m^*/m = (0.13 \pm 0.05)$ for S_1 in the $\Gamma \rightarrow K$ direction. In the $\Gamma \rightarrow M$ direction, $m^*/m = (-0.35 \pm 0.08)$ for S and $m^*/m = (0.14 \pm 0.05)$ for S_1 is found. The given uncertainties are again solely based on the spread of the data. The energetic positions of the two surface states are -243 meV for S and -94 meV for S_1 at Γ in the free-electron dispersion model. For comparison, the results of the relativistic one-step model calculations are shown by the open circles and the dotted lines for an excitation wavelength of 211 nm. Theoretically, effective masses of $m^*/m = -0.33$ for S and $m^*/m = 0.12$ for S_1 are obtained for both directions. Within the experimental limitations the dispersion results in the two directions of the surface Brillouin zone coincide, and match well with the calculated dispersions. The values for the effective electron masses obtained both from experiment and theory are about $m^*/m = 0.13$ for S_1. This value is smaller by a factor of 3 in comparison with earlier IPE measurements.[9] One reason for this could be the smaller $k_\parallel$ interval from which this value is determined in the present work. When considering a larger $k_\parallel$ interval we observe a decrease in curvature, resulting in higher absolute values of the effective masses. Of course, a drastic decrease in curvature is obtained when S_1 is placed at E_F at Γ. This could be the reason in IPE measurements due to insufficient sensitivity at the Fermi energy. An energetical gap of 149 meV between S and S_1 is determined from the separation of the parabolic fit curves. Although the intensity of S vanishes at Γ in the case of the theoretical data, an energetical gap of about 150 meV can be estimated between S and S_1 at Γ when assuming a parabolic form of the dispersion near Γ. Again, experimental and theoretical results agree very well. The earlier mentioned smaller gap of about 120 meV that is achieved when the 1PPE results are treated separately at Γ is probably a more realistic value because of the dependence of the parabolic curves on the chosen $k_\parallel$ interval around Γ. Figure 5 shows that the 1PPE data points for S are above, and for S_1 below, the combined parabolic fit curves, resulting in a smaller gap if considered separately.

Finally, we want to discuss some aspects of the SS forms and widths. At Γ the deduced width for a single surface state is about 160 meV (FWHM). With increasing $k_\parallel$ the signal intensities decrease, and the deduced widths of the surface states increase. 200 meV is observed for a 15° off-normal electron detection for the 1PPE ($k_\parallel \approx 0.11$ Å^{-1}) data, and about 300 meV for the 2PPE ($k_\parallel \approx 0.18$ Å^{-1}) data. This increased width indicates an increasing overlap with the bulk

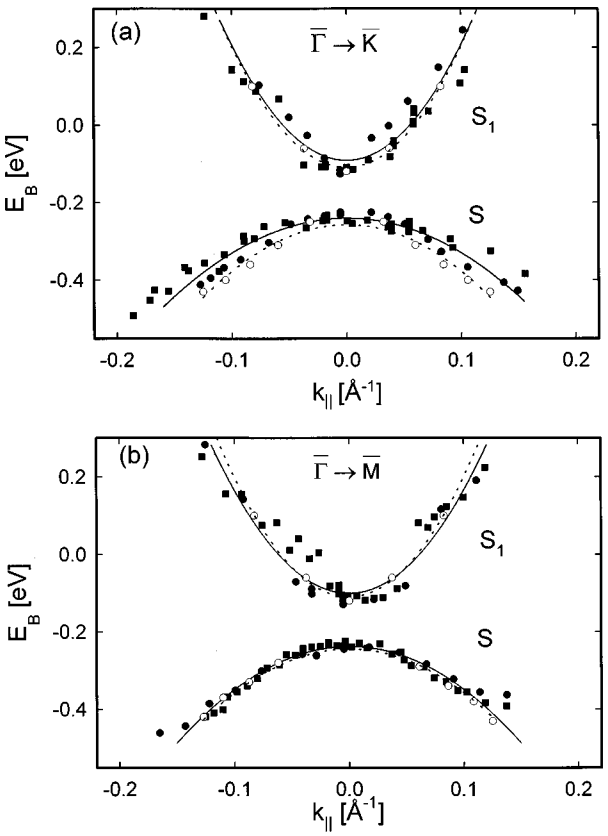

FIG. 5. Dispersion E_B vs $k_{\|}$ for the two observed surface states on Ni(111) for (a) $\bar{\Gamma} \rightarrow \bar{K}$ and (b) $\bar{\Gamma} \rightarrow \bar{M}$ directions. The data points have been obtained by analysis of the measured EDC's with the applied fit model. Results of 1PPE (●) and 2PPE (■) measurements are shown. The data points are fitted by parabolas (continuous lines). The open circles and dashed lines indicate the results of the relativistic one-step model calculations.

states, and, as expected, is most obvious in the 2PPE data. In contrast to Cu and Ag, where narrow surface states are found, on Ni(111) the surface resonances are comparatively broad. These broad resonances are caused by the band structure of Ni(111), where the Fermi level is located within the *d* band. There is no gap around E_F in the (111) direction, and the surface states are degenerate with allowed *d* states except at $\bar{\Gamma}$. Additional, crystal-induced surface states like *S* and S_1 are expected to show spin splittings of the same size as bulk states.[28] An exchange splitting of about 300 meV is reported in the literature from spin-integrated PE measurements for the uppermost *d* band.[6,13,25] A substantial smaller splitting is obtained in spin-resolved IPE measurements for the unoccupied S_1 state, namely, 106 ± 22 meV. This splitting is reported to have the same size as the splitting of the *p*-like gap boundary $L_{2'}$.[7] The lack of spin resolution is a shortcoming in the present high-resolution experiment. The reported spin splitting value and the value obtained for the SS separation at $\bar{\Gamma}$ coincide. Consequently, an interpretation cannot be excluded in which the observed signal structure at $\bar{\Gamma}$ is caused by only one spin-split SS. However, from the development of the PE spectra with increasing $k_{\|}$ (see Fig. 3), we conclude that the given interpretation of two surface states is most reasonable. Applying a curve form analysis of the obtained asymmetric surface states, we estimate a spin splitting to about 70 meV. The energetical separation is less but close to the value reported in spin-resolved IPE measurements. However, a spin-resolved PE experiment with an improved angular resolution is required to confirm this interpretation.

In summary, the analysis of high-resolution photoelectron emission spectroscopy data gives strong evidence for the existence of two crystal-induced surface states on Ni(111) at $\bar{\Gamma}$. Both states are completely occupied and energetically separated by about 120 meV. Theoretical investigations in the framework of the relativistic one-step formalism as well as symmetry considerations need further improvement to explain this experimental result. In contrast, the dispersion of both surface states is well described by the relativistic one-step formalism.

ACKNOWLEDGMENT

The authors would like to thank the Bundesministerium für Forschung und Technologie for partial support of this work under Project No. 13 N 5816.

*Also at Fachbereich Physik, Univesität-GH Essen, D-45117 Essen, Germany.

[1] J. W. Chung, K. S. Shin, D. H. Baek, C. Y. Kim, H. W. Kim, S. K. Lee, C. Y. Park, S. C. Hong, T. Kinoshita, M. Watanabe, A. Kakizaki, and T. Ishii, Phys. Rev. Lett. **69**, 2228 (1992).
[2] K. E. Smith and S. D. Kevan, Phys. Rev. Lett. **64**, 567 (1990).
[3] K. H. Lau and W. Kohn, Surf. Sci. **75**, 69 (1978).
[4] U. Bischler and E. Bertel, Phys. Rev. Lett. **71**, 2296 (1993).
[5] L. E. Urbach, K. L. Percival, J. M. Hicks, E. W. Plummer, and H. L. Dai, Phys. Rev. B **45**, 3769 (1992).
[6] W. Eberhardt, E. W. Plummer, K. Horn, and J. Erskine, Phys. Rev. Lett. **45**, 273 (1980); W. Eberhardt and E. W. Plummer, Phys. Rev. B **21**, 3245 (1980).
[7] M. Donath, F. Passek, and V. Dose, Phys. Rev. Lett. **70**, 2802 (1993).
[8] J. E. Ortega and F. J. Himpsel, Phys. Rev. Lett. **69**, 844 (1992).
[9] F. Passek and M. Donath, Phys. Rev. Lett. **71**, 2122 (1993).
[10] J. E. Ortega, F. J. Himpsel, G. J. Mankey, and R. F. Willis, Phys. Rev. B **47**, 1540 (1993).
[11] K. Garrison, Y. Chang, and P. D. Johnson, Phys. Rev. Lett. **71**, 2801 (1993).
[12] C. Carbone, E. Vescovo, O. Rader, W. Gudat, and W. Eberhardt, Phys. Rev. Lett. **71**, 2805 (1993).
[13] D. E. Eastman, F. J. Himpsel, and J. A. Knapp, Phys. Rev. Lett. **40**, 1514 (1978); F. J. Himpsel and D. E. Eastman, *ibid.* **41**, 507 (1978).
[14] A. Goldmann, M. Donath, W. Altmann, and V. Dose, Phys. Rev. B **32**, 837 (1985).
[15] G. Borstel, G. Thörner, M. Donath, V. Dose, and A. Goldmann, Solid State Commun. **55**, 469 (1985).
[16] E. Bertel, Phys. Rev. B **50**, 4925 (1994).
[17] J. Kutzner, A. Huhmann, and H. Zacharias, Opt. Quantum Electron. **28**, 283 (1996); J. Kutzner and H. Zacharias (unpublished).
[18] J. B. Pendry, Surf. Sci. **57**, 679 (1976).
[19] J. F. L. Hopkinson, J. B. Pendry, and D. J. Titterington, Comput. Phys. Commun. **5**, 599 (1980).
[20] G. Borstel and G. Thörner, Surf. Sci. Rep. **8**, 1 (1988).

[21] M. Grass, J. Braun, and G. Borstel, Phys. Rev. B **47**, 15 487 (1993).
[22] J. Braun, Rep. Prog. Phys. **59**, 1267 (1996).
[23] S. Schuppler, N. Fischer, W. Steinmann, R. Schneider, and E. Bertel, Phys. Rev. B **42**, 9403 (1990).
[24] K. Giesen, F. Hage, F. J. Himpsel, H. J. Riess, and W. Steinmann, Phys. Rev. B **32**, 5241 (1986).
[25] F. J. Himpsel, J. A. Knapp, and D. E. Eastman, Phys. Rev. B **19**, 2919 (1979).
[26] V. L. Moruzzi, J. F. Janak, and A. R. Williams, *Calculated Electronic Properties of Metals* (Pergamon, New York, 1978).
[27] G. Malmström and J. Rundgren, Comput. Phys. Commun. **19**, 263 (1980).
[28] F. Passek and M. Donath, Phys. Rev. Lett. **69**, 1101 (1992).